18th Australasian Fluid Mechanics Conference
Launceston, Australia
3-7 December 2012

Numerical investigation of the stability of model polar vortices in a split-disk system

T. Vo[1], L. Montabone[2] and G. J. Sheard[1]

[1]Department of Mechanical and Aerospace Engineering
Monash University, Victoria 3800, Australia

[2]Atmospheric, Oceanic and Planetary Physics
University of Oxford, Parks Road, Oxford OX13PU, United Kingdom

Abstract

The stability of a rotating system differentially forced at the lid and base of a cylindrical enclosure is numerically investigated. The shear layer arising from the angular velocity discrepancy at the disk-tank interface becomes unstable beyond a threshold of two governing parameters known as the Rossby number *Ro*, and Ekman number Ek. Beyond the threshold of instability, the shear layer deforms into a chain of vortices configured into a polygonal pattern which precesses around the central axis. The number of vortices depends on *Ro* and Ek.

The incompressible Navier–Stokes equations are solved on a two-dimensional meridional semi-plane. A linear stability analysis of the steady-state axisymmetric flow solutions is performed to determine the most unstable azimuthal modes, which are mapped onto an *Ro*-Ek regime diagram. In contrast to laboratory observations in a similar system, it is found that Ek and the sign of *Ro* have a strong influence on the preferential mode.

Introduction

Rotating flows are renowned for the interesting structures that they exhibit and are widely observed in practical applications and geophysical phenomena. The extensive range of structure scales are exploited by reproducing strikingly similar configurations to large-scale atmospheric structures at a laboratory scale. Of particular interest are the types of instabilities acting on the shear layers in these rotating flows which develop coherent vortices that rearrange themselves into polygonal shapes. These structures are representative of the massive polar vortices on planets, such as Saturn's hexagonal North Polar vortex and Venus' dipolar South polar vortex. Barotropic instability, which is related to the horizonal shear, has been of interest in producing these visually aesthetic structures and may be the cause of existing polar vortices [1, 9].

A rotating cylinder coupled with differentially rotating disks induces Stewartson layers to form across regions of discontinuous azimuthal forcing. This shear layer serves to smooth out the discontinuity in angular velocity across the layer and becomes unstable under certain and reproducible conditions. Three dimensionless governing parameters characterizing these flows are the Rossby number, Ekman number and the Reynolds number. The Rossby number (*Ro*) represents the ratio between inertial and Coriolis forces, the Ekman number (Ek) as the ratio between viscous and Coriolis forces and the Reynolds number (*Re*) is the ratio between inertial and viscous forces in a flow. Large-scale atmospheric and oceanic flows typically have magnitudes of Rossby and Ekman numbers much less than unity, indicating a high importance of rotation on the dynamics of the system.

At the onset of instability, the initially circular shear layer begins to roll up and form a ring of multiple vortices. Experimental studies [1, 5, 6] have all exhibited a decrease in the number of vortices with an increase in the parameter values beyond the stability threshold, despite geometric and forcing differences.

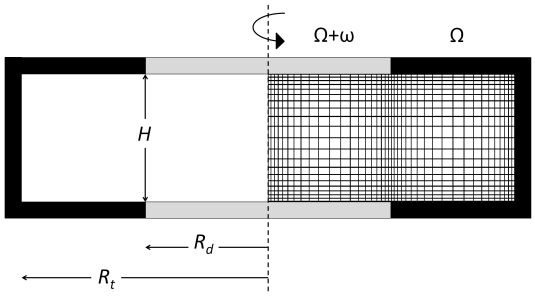

Figure 1: Meridional plane of the system under investigation. The grey shaded regions represent the disks which rotate at a rate of $\Omega+\omega$ while the black shaded regions represents the tank which rotates at Ω. The right semi-plane illustrates the spatially discretized mesh used for the numerical simulations. The dimensions shown here are not to scale.

This trend is consistently observed in shear layer experiments and has also been observed in simple numerical models [4, 8]. This is in contrast with linear stability results from [10] which found an increase in the number of vortices with increasing *Re*. Differences are also seen between positive and negative *Ro* in relation to the flow states available. In [6], only an off-axis ellipse is observed for negative *Ro* and wavenumbers 2 to 6 for positive *Ro*. However, a study by [5] managed mode transitions to lower modes with increasing *Ro* magnitude for both negative and positive *Ro*.

This paper considers a differential rotating system closely following [1] and [5]. The system is comprised of a rotating cylindrical tank with disks located at the base and lid which rotate at a different angular velocity. This system differs from the experimental set-up through the absence of a central rod used to drive the rotation of the disks. Thus, this set-up produces flows which eliminates any external disturbances which may otherwise be introduced into the system. A three-dimensional model of this configuration is used to investigate the linear stability of the flow for both positive and negative *Ro*. This investigation differs from previous numerical studies which have mainly considered two-dimensional quasi-geostrophic models where quantitative discrepancies and flow state limitations may be present. As a consequence, details of the vertical flow structure are scarce.

Methodology

Problem definition

The system comprises of a closed cylindrical tank of radius R_t and height H. Two disks of radius R_d are located at the base and lid of the tank which rotate at a different rate to that of the tank. The tank rotates at a rate of Ω while a differential rate of ω are imposed on the disks. Thus, negative and positive

ω indicates the disks rotating slower and faster than the tank, respectively. A schematic diagram of the investigated model is shown in figure 1. The tank is filled with an incompressible Newtonian fluid.

Governing Equations

The lengths, velocities, time and pressure are normalized by R_d, $R_d\Omega$, $1/\Omega$ and $R_d\Omega^2\rho$, respectively, where ρ is the fluid density. The flow in this system is governed by the unsteady incompressible Navier–Stokes equations given in non-dimensional form as

$$\begin{aligned} \frac{\partial \mathbf{u}}{\partial t} + (\mathbf{u}\cdot\nabla)\mathbf{u} &= -\nabla P + \frac{EkA^2}{1-ARo}\nabla^2\hat{\mathbf{u}}, \\ \nabla\cdot\mathbf{u} &= 0, \end{aligned} \tag{1}$$

where $\mathbf{u} = (u_z, u_r, u_\theta)$ is the velocity vector, P is the kinematic pressure, $A = H/R$ as the aspect ratio, Ro the Rossby number and Ek as the Ekman number. The Rossby and Ekman number are defined as

$$Ro = \frac{R\omega}{2\overline{\Omega}H}, \quad Ek = \frac{\nu}{\overline{\Omega}H^2}, \tag{2}$$

where $\overline{\Omega} = \Omega + \omega/2$ is the mean fluid rotation following [5]. A negative and positive Ro signifies the disk rotating slower and faster than the tank rotation, respectively. The choice of reference scales affects the governing equations as seen in equation (1) where the diffusion coefficient contains a singularity. The dependence of Ro in the denominator of this diffusion coefficient term dictates the availability of computable Ro space in this paradigm as the term can neither be zero or negative. Thus for $A = 2/3$, only $Ro < 3/2$ can be analysed which is sufficient for this study. Alternative paradigms can be generated with different reference scales, allowing higher Ro to be investigated.

Numerical Treatment

The base flow is assumed to be axisymmetric and is computed on a meridional semi-plane. The spatially discretized mesh is shown in figure 1. Three distinct boundary conditions are implemented on the mesh. Boundaries shaded grey rotate at $\Omega+\omega$ while the black boundaries rotate at Ω. The dashed line represents the axis of symmetry and rotation which is treated with a symmetry boundary condition similarly to [3].

Each macro element has an imposed polynomial degree of order N_p. The order N_p determines the spatial resolution of the domain. The governing equations are solved in cylindrical coordinates through a spectral-element discretization in space and a third-order time-integration scheme based on backward differentiation [7]. Optimization between computational resources and solution accuracy has been achieved with $N_p = 11$. This was measured through convergence tests of three global parameters which demonstrated an error of less than 0.1% at the nominated N_p. Thus, $N_p = 11$ has been implemented in all simulations reported herein.

Non-axisymmetric three-dimensional instability modes are computed via a linear stability analysis. The technique used follows [2, 11] where the axisymmetric base flow and the three-dimensional perturbation fields are decoupled. Each perturbation field of a specific wavenumber in the azimuthal direction is not influenced by other wavenumbers. The steady-state base flow solution is supplied to the evolving perturbation fields, which are governed by the linearized Navier–Stokes equations. The leading eigenmodes of the flow are determined; the eigenvalues relate to the Floquet multipliers of the system and the eigenvectors characterize the mode shape of the perturbation field. The Floquet multiplier μ_f is related to the growth rate σ via $\mu_f = e^{\sigma T}$ where T is an arbitrary time interval over which the equations are integrated within the eigenmode solver. Thus, $|\mu_f| < 1$ represents a stable flow and $|\mu_f| > 1$ an unstable flow, where growth rates are negative and positive, respectively.

(a) Positive Ro

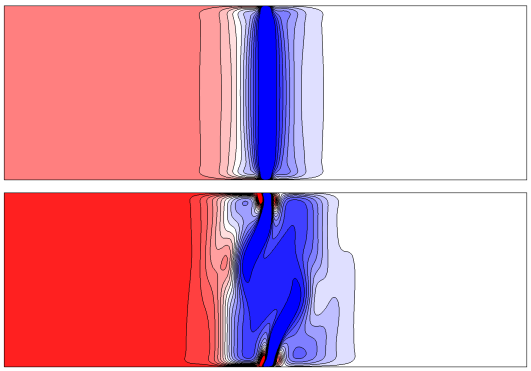

(b) Negative Ro

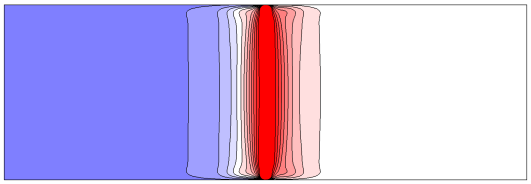

Figure 2: Contour plots of axial vorticity for flows of $Ek = 5 \times 10^{-4}$ for (a) $Ro = 0.01$ (top) and $Ro = 0.5$ (bottom) and (b) $Ro = -1.0$. Blue to red contours show arbitrary low and high values, respectively.

Results and Discussion

Axisymmetric flow

The Rossby and Ekman numbers investigated here range between $-1.5 < Ro < 0.5$ and $5\times10^{-5} < Ek < 4.5\times10^{-3}$. A pairing of these two parameters is used to define the flow.

For small Rossby numbers, the flow exhibits highly two-dimensional features in the vertical where motions are suppressed along the axis of rotation. This is illustrated in the top panel of figure 2(a) through the vertical contour lines of axial vorticity. The azimuthal velocity contours (not shown here) also depict depth-independent contours representative of solid-body rotation. As positive Ro is increased, the differences between the azimuthal forcing velocities become large and the symmetry of the flow is broken as depicted in the bottom panel of figure 2(a). Evidently the contour lines are distorted. An initial patch of negative vorticity arising at the disk-tank interface grows into strands which extend into the flow interior. Further increases causes the negative vorticity strands to elongate and lose their vertical symmetry. The vorticity is positive everywhere else.

The flow behaviour differs between negative and positive Rossby number. For the range of negative Ro investigated here, the motions exhibited reflective symmetry about the horizontal mid-plane. A flow with $Ro = -1.0$ is shown in figure 2(b). The negative vorticity patch present in positive Ro is not observed at negative Ro. Also, Ekman pumping and suction is evident in positive and negative Ro flows, respectively. As the disks rotate faster than the tank, fluid is drawn radially towards the disk-tank interface which is then expelled axially into the flow interior.

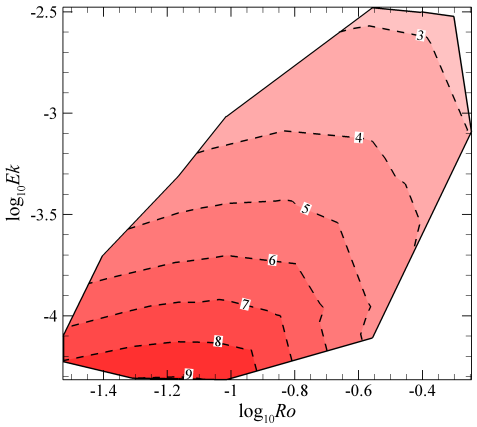

Figure 3: The regime diagram of the most unstable linear modes as a function of Ek and positive Ro. The dashed lines represents the transition between one mode to another, denoted by the wavenumber of the instability shown. The solid boundary lines represents the range of triangulation.

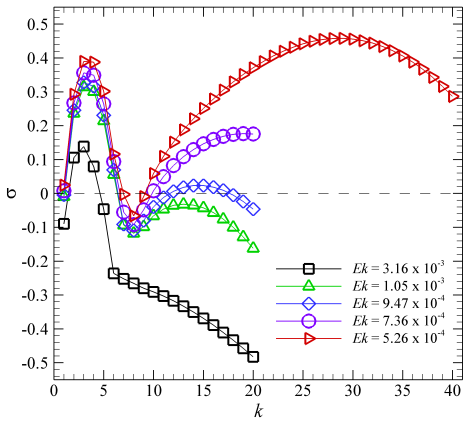

Figure 4: Growth rate σ as a function of wavenumber k for various Ek at $Ro = 0.395$. Two peaking structures of σ are present at low and high wavenumbers. The dashed line represents the zero-line where points above and below symbolize stable and unstable modes, respectively.

Linear Stability Analysis

The growth rates for a range of azimuthal wavenumbers defined by $k = 2\pi/\lambda$ are obtained which expresses the stability of the modes and reveals the fastest-growing instability mode. Here, angle λ denotes the azimuthal wavelength. The wavenumbers range between $1 < k < 20$ and the eigenvalues are consistently quasi-periodic. A selected wavenumber perturbation field is evolved on a steady-state base flow characterized by Ro and Ek.

Unstable modes ranging primarily from wavenumbers 3 to 9 are observed for positive Ro. The preferential unstable modes have a tendency to decrease with increasing Ro and also with increasing Ek. An Ro-Ek regime diagram of the most unstable wavenumber is shown in figure 3. The experimental studies from [1, 5] also observe these trends and obtained wavenumers 2 to 8. However the experimental trends depict a stronger dependence on Ro compared to Ek. In contrast, the numerical results demonstrate a strong dependence on Ek below a particular Ro and beyond that, the dependence of the most unstable mode is shifted to Ro.

For low Ro or high Ek, the growth rate against wavenumber profile is depicted by a single mode peak as seen in figure 4 for $Ek = 3.16 \times 10^{-3}$. However, a second mode peak at higher wavenumbers begins to emerge as Ro is increased or Ek is decreased beyond a certain threshold. This eventually causes the higher wavenumbers of the second peak to exhibit the largest growth rates. This suggests that short-wavelength structures will emerge in the flow. The growing of the second mode peak structure with decreasing Ek is demonstrated figure 4. For $3.16 \times 10^{-3} \leq Ek \leq 7.36 \times 10^{-4}$, the unstable wavenumber of the flow is $k = 3$. As the Ekman number is decreased to $Ek = 5.26 \times 10^{-4}$, the leading unstable wavenumber increases suddenly from $k = 3$ to $k = 29$. It is unclear whether these higher modes are observed in the experiment. The emergence of this high-wavenumber mode may promote the "chaotic" regime observed in the laboratory [1]. These higher wavenumbers are not included in figure 3 and will be described in a forthcoming paper.

Differences are seen between positive and negative Ro. For negative Ro the range of unstable wavenumbers observed is between 3 and 12. Experimental work by [5] also studied negative Ro which only obtained wavenumbers 2 to 8. Unlike results of linear stability analysis for positive Ro, only a single peaking structure is seen to exist. For increasing Ro magnitude or decreasing Ek, the growth rate continues to increase and shifts the most unstable wavenumber to higher modes. Experimental results of [5] report similar trends for negative and positive Ro where modes decrease with either increasing Ro or Ek. This is in contrast to the numerical results as shown in the regime diagram in figure 5. It demonstrates an increase in unstable mode for increasing Ro magnitude with a weak dependence on Ek.

The threshold of stability of Ro as a function of Ek differs between positive and negative Ro. Growth rates are obtained by scanning through the Ro and Ek parameter space. A growth rate value of zero is then obtained via triangulation along with the corresponding Ro and Ek threshold value. The critical Rossby number obtained from an empirical fit follows the relationship given by $|Ro_c| \propto Ek^{0.767}$ for positive Ro, and $|Ro_c| \propto Ek^{0.826}$ for negative Ro. These relationships differ from the one obtained in [5], given by $|Ro_c| = 27Ek^{0.72}$. Data points from negative and positive Ro were used to obtain this empirical fit as no differences were found between negative and positive Ro thresholds. These discrepancies may be due to the presence of the rod which drives the disks or the experimental flow may contain non-linear effects which are neglected in this analysis.

Despite the differences in stability trends between negative and positive Ro, the instability mode shape and vertical structure is primarily consistent. The structure of the instability mode is vertically independent similar to its basic flow. The three-dimensional flow is reconstructed from a spectral-element-Fourier expansion of a superposition of the two-dimensional base flow and the leading eigenmode of an instability. An instability structure of $k = 5$ at mid-depth is shown in figure 6. This mode exhibits a pentagonal configuration which does not change throughout the vertical except for regions near the horizontal boundaries. The circumferential chain of vortices is comprised of higher vorticity compared to the central polar vortex for negative Ro and reversed for positive Ro. Other polygonal shapes have also been captured such as triangles ($k = 3$), squares ($k = 4$) and hexagons ($k = 6$). A distinct polygonal configuration is more difficult to observe with higher wavenumbers due to the shorter wavelengths forming around the disk.

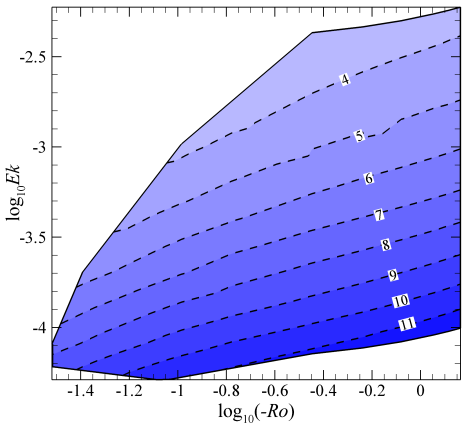

Figure 5: The same as figure 3 except for negative *Ro*.

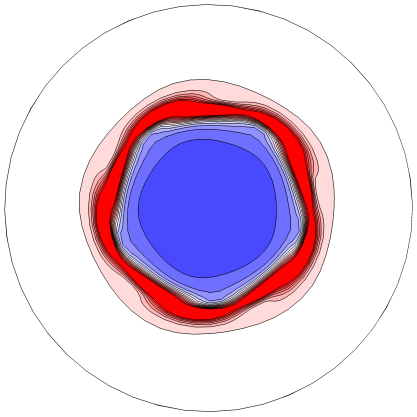

Figure 6: Flooded contours of the vertical vorticity of a wavenumber-5 mode of $Ro = -0.357$ and $Ek = 1.29 \times 10^{-3}$. The vorticity field shown is at mid-depth and is the superposition of the global linear instability mode shape of 5 and the underlying axisymmetric base flow. This mode exhibits a pentagonal configuration. Blue to red contours show arbitrary low and high values, respectively.

Conclusions

A numerical study on the linear stability of flows generated in a rotating cylindrical tank with differential boundary forcing has been conducted. Axisymmetric flows characterized by a pair of *Ro* and Ek values were obtained. Low *Ro* flows exhibit features indicative of the Taylor-Proudman theorem where flows are highly two-dimensional with motions suppressed along the axis of rotation. As positive *Ro* is increased, the flow loses its two-dimensional nature and becomes complex in structure. Increases in negative *Ro* magnitude continues to display vertical independence.

Linear stability analysis revealed two distinct modes in plots of growth rate against wavenumber for positive *Ro*. One mode emerges at low wavenumbers and is the dominant mode at low *Ro* and high Ek. With increasing *Ro* or decreasing Ek, the second mode outgrows the first indicating that a higher wavenumber governs the flow. This dominant higher wavenumber may be related to irregular and chaotic flows seen in experimental studies. In the negative-*Ro* regime, only a single instability mode was detected.

Differences in stability properties are seen between positive and negative *Ro*. The peak wavenumbers of instabilities in the positive-*Ro* regime exhibited strong dependence on both *Ro* and Ek, whereas a weak dependence on *Ro* is displayed for negative *Ro*. The threshold of stability also differed between negative and positive *Ro* which is in contrast to that reported by [5]. The discrepancies may be due to the absence in these simulations of the central rod present in [5], and the absence of non-linear mode evolution in the present analysis.

Acknowledgements

This research is supported by the Australian Research Council through Discovery Grant DP120100153 and by the Monash University Faculty of Engineering Seed Funding Scheme. Numerical work has been conducted on the high performance computing facility, Monash Sun Grid, and supplemented by the support of a grant under the NCI Merit Allocation Scheme.

References

[1] Aguiar, A.C.B., Read, P.L., Wordsworth, R.D., Salter, T. and Hiro Yamazaki, Y., A laboratory model of Saturn's North Polar Hexagon, *Icarus*, **206 (2)**, 2010, 755–763.

[2] Barkley, D. and Henderson, R.D., Three-dimensional Floquet stability analysis of the wake of a circular cylinder, *Journal of Fluid Mechanics*, **322**, 1996, 215–241.

[3] Blackburn, H.M. and Sherwin, S.J., Formulation of a galerkin spectral element-Fourier method for three-dimensional incompressible flows in cylindrical geometries, *Journal of Computational Physics*, **197 (2)**, 2004, 759–778.

[4] Chomaz, J.M., Rabaud, M., Basdevant, C. and Couder, Y., Experimental and numerical investigation of a forced circular shear layer, *Journal of Fluid Mechanics*, **187 (1)**, 1988, 115–140.

[5] Früh, W.G. and Read, P.L., Experiments on a barotropic rotating shear layer. Part 1. Instability and steady vortices, *Journal of Fluid Mechanics*, **383**, 1999, 143–173.

[6] Hide, R. and Titman, C.W., Detached shear layers in a rotating fluid, *Journal of Fluid Mechanics*, **29**, 1967, 39–60.

[7] Karniadakis, G.E., Israeli, M. and Orszag, S.A., High-order splitting methods for the incompressible Navier–Stokes equations, *Journal of Computational Physics*, **97 (2)**, 1991, 414–443.

[8] van de Konijnenberg, J.A., Nielsen, A.H., Juul Rasmussen, J. and Stenum, B., Shear-flow instability in a rotating fluid, *Journal of Fluid Mechanics*, **387**, 1999, 177–204.

[9] Montabone, L., Wordsworth, R., Aguiar, A., Jacoby, T., McClimans, T., Read, P.L. and Wilson, C., Coherent structures in planetary polar vortices: A laboratory view, International Conference on Comparative Planetology: Venus-Earth-Mars, ESTEC, 2009.

[10] Niino, H. and Misawa, N., An experimental and theoretical study of barotropic instability, *Journal of Atmospheric Sciences*, **41**, 1984, 1992–2011.

[11] Sheard, G.J., Wake stability features behind a square cylinder: Focus on small incidence angles, *Journal of Fluids and Structures*, **27**, 2011, 734–742.